JOURNAL OF MARITIME RESEARCH

Vol XXII. No. II (2025) pp 80–86

ISSN: 1697-4840, www.jmr.unican.es

Numerical Investigation of Validation and Verification for the Resistance of JBC Hull

Md Mehrab Khan[1], Sajib Das[1,*], Md. Mashud Karim[1]

ARTICLE INFO

Article history:
Received 12 Aug 2024;
in revised from 20 Aug 2024;
accepted 17 Sep 2024.

Keywords:
Validation, FVM, STAR-CCM+, VOF, Uncertainty.

ABSTRACT

Regarding the purpose of determining the hydrodynamic properties of ships, the potential uses of computational fluid dynamics (CFD) have been performing significant progress. The prediction of resistance is one of the several task that is considered to be among the most essential components when designing a ship. The present study involves conducting numerical simulations in STAR-CCM+ to determine the resistance and resistance coefficient produced by the Japan Bulk Carrier (JBC) hull in calm water condition. There is also an investigation into the verification and validation processes that are carried out using three distinct grids that have been precisely refined. The numerical findings of the study that are very similar to the experimental findings arising from the towing tank model evaluation. Through current numerical approaches and grid distribution are capable of effectively predicting fluid flow region that is sufficient to encompass JBC hull since wave patterns provide an accurate representation of Kelvin wave patterns. In addition, the uncertainty of the comparison is lower than the uncertainty of the validation which implies that the validation has been effectively achieved.

1. Introduction.

Computational fluid dynamics (CFD) is employed for geometry and physics that are becoming increasingly complicated and is being incorporation within the procedures of technological design, due to the pressing nature of the situation, progress have intensified to achieve agreement on the terms and ideas as well as methodological approaches that are practical. Computational Fluid Dynamics methods have experienced significant growth in recent years. This can be attributed to the improved computational capabilities and the expanded application of the Navier-Stokes equation to more intricate physical challenges. As a result, it has become feasible to solve difficulties involving several stages as well as free surfaces flows [Gaggero, et al., 2015]. Through the use of Computational Fluid Dynamics (CFD), analysis of ships hydrodynamic performance, which includes calm water resistance, seakeeping, and maneuverability, is often accomplished [Khan, et al., 2019]. In order to find the resistance of a ship within calm water, Niklas and Pruszko evaluated techniques based on numerical along with experimental data [Niklas & Pruszko, 2019]. Zhao et al. investigated the flow of viscous fluid surrounding the hull along with a free surface by dealing with the Reynolds-averaged Navier-Stokes (RANS) equations [Zhao, et al., 2005]. However, conducted computer simulations of the viscous flow surrounding a tanker hull in order to calculate the overall resistance is conducted by Farkas et al. [Farkas, et al., 2017]

In terms of Validation and Verification, the Richardson Extrapolation (RE) process is the foundation for almost every one of the suggested processes where convergence is investigated using grids that have been refined in a systematic manner [Richardson, 1911]. Verification is the procedure of identifying if the equations have been solved accurately, whereas validation is the procedure of discovering if the appropriate equations have been solved [Roache, 1998]. During the verification process, the principal cause of numerical inaccuracy arises from both iteration and discretization. However, the overwhelming factor contributing to this inaccuracy is the discretization process. On

[1]Department of Naval Architecture and Marine Engineering, Bangladesh University of Engineering and Technology, Dhaka-1000, Bangladesh.
[*]Corresponding author: Sajib Das. E-mail Address: sajibdas005@gmail.com.

the contrary, validation assesses the level of precision at which the computational model represents the actual physical situation in conjunction with the experimental fluid dynamics (EFD) results.

This investigation aims to calculate the resistances and the total resistance coefficient of the Japan Bulk Carrier (JBC) hull in calm water condition at Froude Number 0.142. Furthermore, a standard Verification and Validation (V&V) procedure is utilized to regulate and comprehend the models and numerical inaccuracies in the calculations. The simulation is conducted using the commercial system STAR-CCM+ in this investigation. The initial steps commenced with the establishment of coordinate framework to develop the computational domain, and the specification for boundary conditions. The *k–ε* turbulence model which has been employed for encapsulating RANS equations. Volume of Fluid (VOF) approach is utilized for accurately representing and track the interface between two fluids, specifically capturing the free surface. The grid convergence study relies on three distinct sets of sequentially refined grids.

2. Numerical Background.

The Reynolds-Averaged Navier-Stokes (RANS) equations are utilized as governing equations for the modelling of an unstable incompressible viscous flow with two phases field. The RANS and VOF equations are converted into computational form and discretized by the application of the finite volume method (FVM). In contrast, governing equations that can be utilized for solving the difficulty of an unsteady, three dimensional, and viscous flow. The continuity equation and momentum equation are expressed as [Yu, et al., 2019]:

Continuity Equation:

$$\nabla \cdot \boldsymbol{U} = 0$$

Momentum Equation:

$$\frac{\partial \rho U}{\partial t} + \nabla \cdot \left(\rho \left(U - U_g\right) U\right) = -\nabla p_d - g \cdot x \nabla \rho + \nabla \cdot \left(\mu_{eff} \nabla U\right) + (\nabla U) \cdot \nabla \mu_{sff} + f_\sigma + f_s$$

The variables in the equation are defined as follows: U denotes the velocity of the fluid, U_g indicates the velocity of the grid, p_d refers the dynamic pressure, ρ is mixed the density of the multiphase and g signifies the acceleration due to gravity. The effective dynamic viscosity, expressed as μ_{eff}, can be calculated as the sum of $(\nu + \nu_t)$, where ν denotes the kinetic viscosity and ν_t indicates the eddy viscosity. The surface tension term is denoted by f_σ, which influence can be detected on the free surface and the source term is defined by *fs* that is a sponge layer is incorporated for efficiently absorbing the created wave.

For the purpose of dealing with the interface between multiphase, Volume of Fluid (VOF) approach with constrained compression is utilized [Weller, 2008]. Through the process of resolving an advection equation, it's possible to ascertain the volume fraction function. The general transpose equation is given below:

$$\frac{\partial \alpha}{\partial t} + \nabla \cdot \left[\rho \left(U - U_g\right) \alpha\right] + \nabla \cdot \left[U_r \left(1 - \alpha\right) \alpha\right] = 0$$

In the Volume of Fluid (VOF) approach, each phase of the two-phase system is assigned a distinct volume fraction (α). A value of 0 represents the presence of air in the cell, while a value of 1 represents the presence of water. A value between 0 and 1 indicates the interface between the two-phase fluid. U_r is the field of velocities employed for interface compression.

The *k–ε* turbulence model is utilized in this investigation to predict the average flow properties in turbulent flow conditions having a greater accuracy. The *k–ε* turbulence model is a type of eddy viscosity model that consists of two equations. The k-ε model utilizes the transport equations [Versteeg and Malalasekera (2006)] that are provided below, where k represents the turbulent kinetic energy and ε represents the dissipation rate of the energy produced.

$$\frac{\partial(\rho k)}{\partial t} + \mathrm{div}(\rho k \boldsymbol{U}) = \mathrm{div}\left[\frac{\mu_t}{\sigma_k} \mathrm{grad} k\right] + 2\mu_t S_{ij} \cdot S_{ij} - \rho\varepsilon$$
$$\frac{\partial(\rho\varepsilon)}{\partial t} + \mathrm{div}(\rho\varepsilon \boldsymbol{U}) = \mathrm{div}\left[\frac{\mu_t}{\sigma_\varepsilon} \mathrm{grad}\varepsilon\right] + C_{1\varepsilon}\frac{\varepsilon}{k} 2\mu_t S_{ij} \cdot S_{ij} - C_{2\varepsilon}\rho\frac{\varepsilon^2}{k}$$

The variable μ_t indicates the eddy viscosity, while σ_ε *and* σ_k are Prandlt numbers. The variable S_{ij} depicts the rate of deformation.

3. Geometry.

The following figure displays the geometric structure of the bulk carrier model. Additionally, Table 1 provides a comprehensive description of the ship's features as well as the details of the model.

Figure 1: Geometry of JBC Hull.

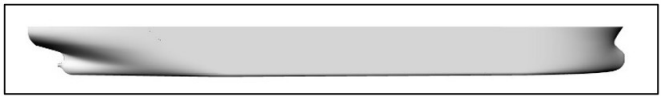

Source: Authors.

The table provided, Table 1, contains the principal dimensions and details of JBC hull and the scale ratio is 1:40.

Table 1: Principal particulars of JBC Hull.

Principal Particulars		Full Scale	Model Scale
Length Between Perpendiculars	L_{PP} (m)	280	7.00
Beam of Waterline	B_{WL}(m)	45	1.125
Depth	D (m)	25	0.625
Draft	T_M (m)	16.5	0.4125
Displacement	∇ (m^3)	178369.9	2.7872
Wetted Surface Area	S_0 (m^2)	19556.1	12.222
Block coefficient	C_B	0.858	0.858
Moment of Inertia	K_{xx}/B	0.4	0.4
Moment of Inertia	K_{yy}/L_{PP}	0.25	0.25
Moment of Inertia	K_{zz}/L_{PP}	0.25	0.25

Source: Authors.

For the purpose of the resistance test, the water conditions were kept calm throughout the process. The current investigation of the main body of the ship is being carried out using a numerical simulation, using the accurate model hull speed of 1.179 m/s at Froude Number 0.142 and because of symmetry, just half of the model is simulated. The experimental data had been obtained through the CFD workshop that took place in Tokyo in 2015 [Hino, et al., 2020].

4. Computational Domain and Boundary Conditions.

A computational domain is utilized for numerical simulation, with the domain expanding in three orthogonal directions: -3.0 Lpp < X < 2.57Lpp, 0 < Y < 2.57Lpp, and -1.285Lpp < Z < 2.57Lpp.

Figure 2: Computational Domain.

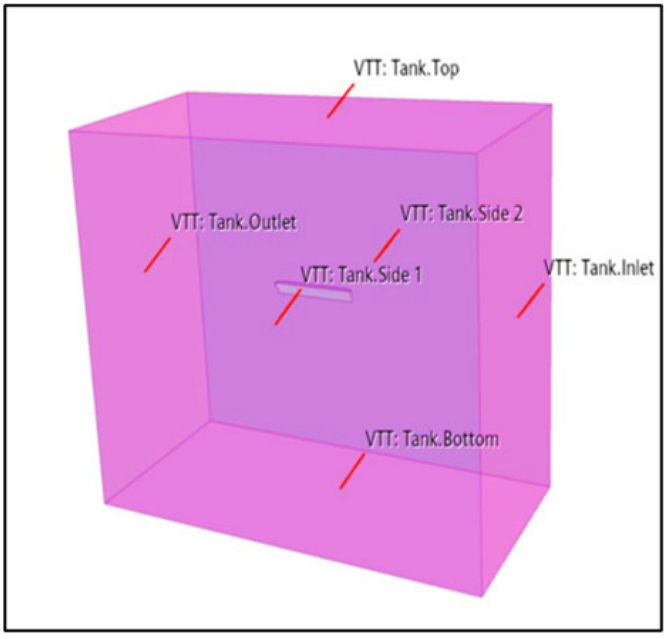

Source: Authors.

As shown in Figure 2, all of the domain's faces have had the following boundary conditions applied to them as well as the surface of the hull. For the hull, it has been specified as wall, which signifies the no slip conditions.

Table 2: Boundary Conditions of the Domain Faces.

Boundary	Boundary
Tank.Top	Velocity Inlet
Tank.Bottom	Velocity Inlet
Tank.Outlet	Pressure Outlet
Tank.Inlet	Velocity Inlet
Tank.Side 1	Symmetry Plane
Tank.Side 2	Symmetry Plane

Source: Authors.

5. Mesh Generation.

Three grids were used throughout the simulation, and each grid had been generated with a separate base mesh size. This method for creating meshes makes use of a Trimmed cell mesher as well as a prism layer mesher around the margins of walls for improving the precision of the resolution of boundary layer when it was in close proximity to solid objects. For the purpose of reproducing standard flow patterns in turbulent flow circumstances, the k - ε Turbulence model with all y+ layers treatment provides the necessary framework. The subsequent illustration displays detailed grid distributions.

Figure 3: Mesh Distribution around (a) Domain (b) Hull.

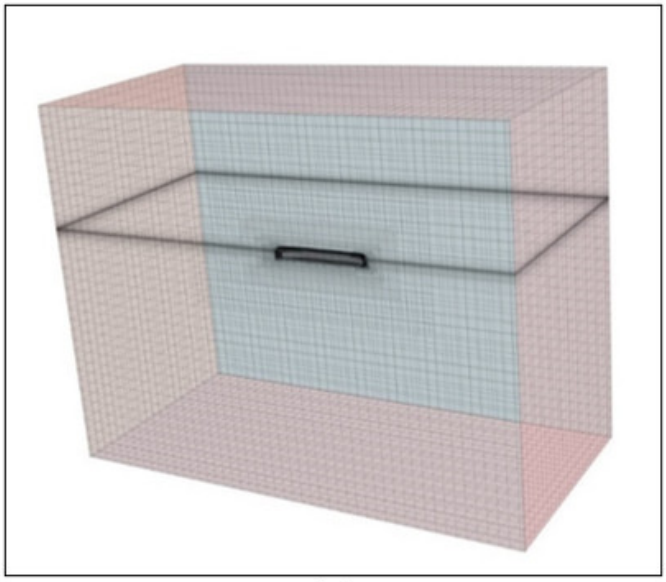

(a)

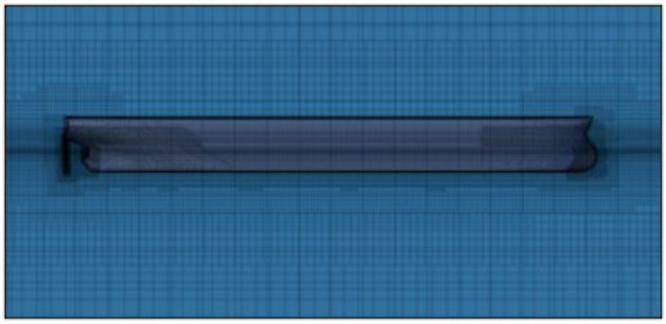

(b)

Source: Authors.

The mesh refinement that was performed in order to effectively capture the free surface in addition resemble the Kelvin wake pattern of the JBC model.

Figure 4: Mesh Refinement (a) Isometric View (b) at Free Surface.

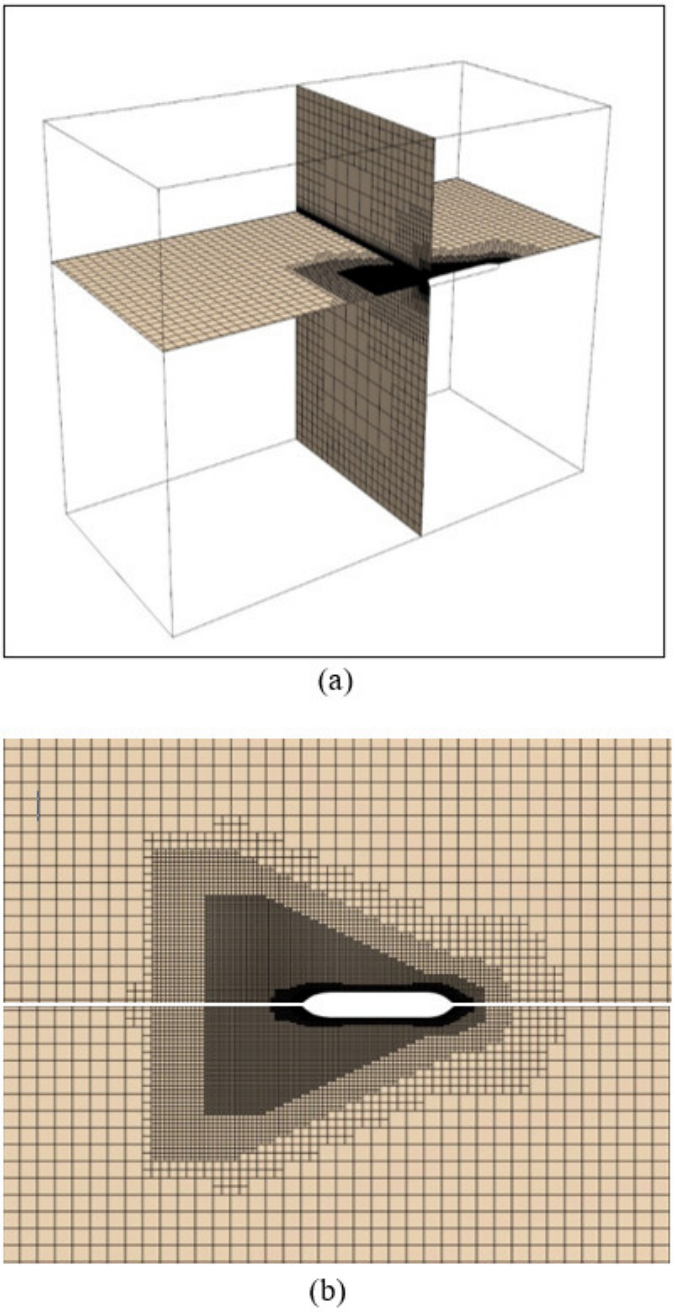

Source: Authors.

6. Results and Discussion.

In the implicit unsteady solver, the physical time step is chosen in accordance with the ITTC guideline, which results in the mathematical formulation that is $\Delta t = 0.005 \sim 0.01$ L/U [ITTC, 2011]. The time step is denoted by Δt, the length between perpendiculars is denoted by L, and the flow velocity is denoted by U. Within the simulations, a time step of 0.04 seconds was utilized throughout the process. For grid independence study, the total resistance that was acquired at Froude Number 0.142 for each of the different grids is displayed below.

Table 3: Grid Independence Study at Froude Number 0.142.

Grid	Base Size (m)	Cell Numbers	Resistance (N)
Coarse	0.125	449147	35.54
Medium	0.1125	526195	35.98
Fine	0.1	660820	36.02

Source: Authors.

The results of comparative analysis of the Resistance Coefficient with the results of CFD as well as EFD [Hino, et al., 2020] at Froude number 0.142 are shown below.

Table 4: Comparative Study of CFD and EFD results at Froude Number 0.142.

Grid	$C_T \times 10^3$ (CFD)	$C_T \times 10^3$ (Exp. by Hino et al., 2020)	Deviation (%)
Coarse	4.184	4.29	2.47
Medium	4.236		1.27
Fine	4.240		1.16

Source: Authors.

The overall resistance coefficient that yields the best results is 4.24×10^{-3}, which additionally appears to have the lowest deviation of 1.16%.

The provided figure illustrates the free surface generated by the hull at a Froude number of 0.142.

Figure 5: Free Surface.

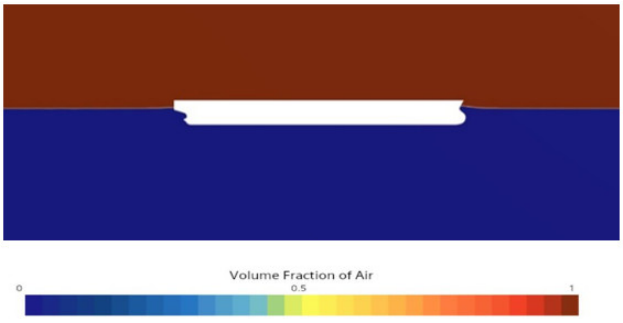

Source: Authors.

The following graphic depicts the wave patterns formed by the hull at Froude number 0.142.

Figure 6: Wave Patterns around the Hull (a) Top View (b) Isometric View.

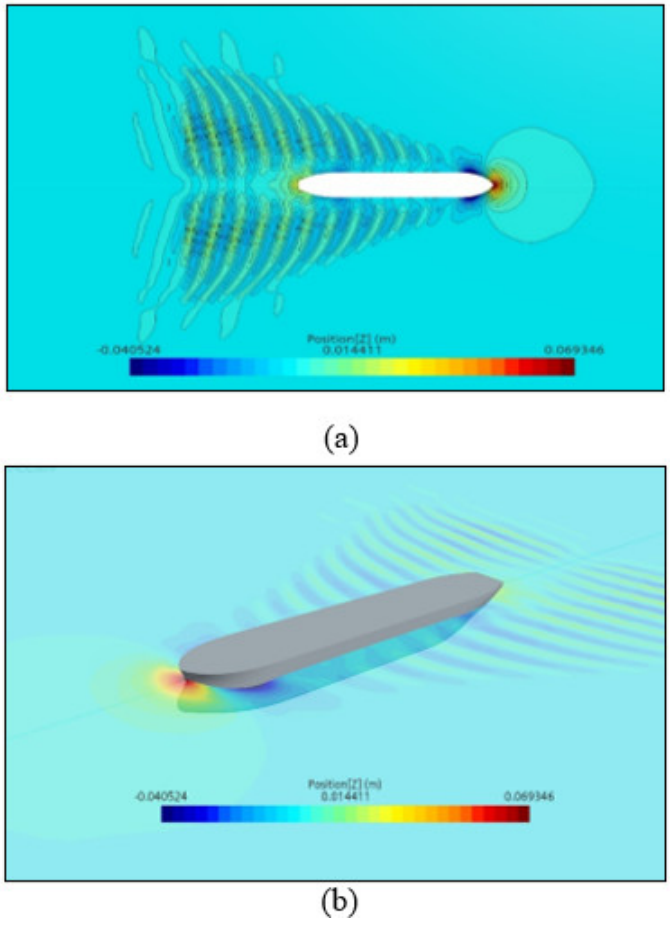

Source: Authors.

The provided figure illustrates the hull's pressure distribution at Froude number 0.142.

Figure 7: Pressure Distribution around the hull.

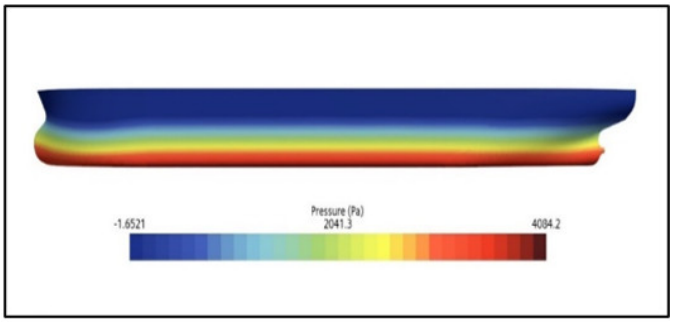

Source: Authors.

The picture that has been provided contains an illustration of the velocity contour of the hull at Froude number 0.142.

Figure 8: Velocity Contour around the hull.

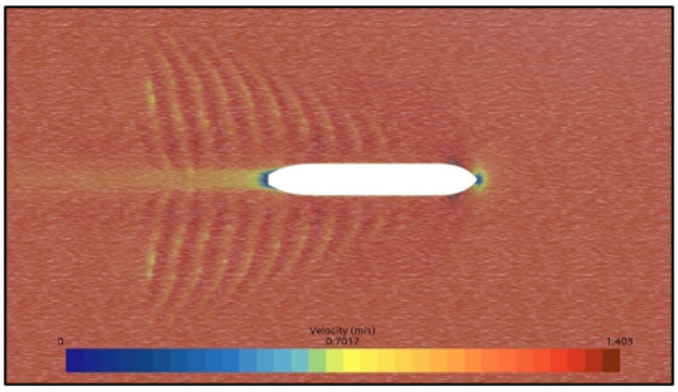

Source: Authors.

Finally, A comparison is made between the measurement of wave elevation on JBC Hull Surface and the outcomes from the experiment [Hino, et al., 2020] at Froude Number 0.142 in the accompanying figure.

Figure 9: Comparison of Wave Elevation.

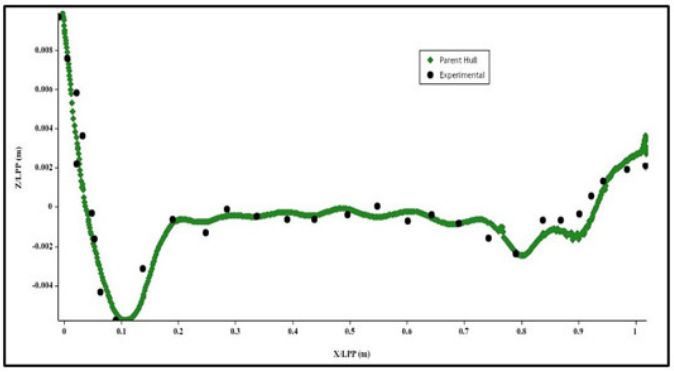

Source: Authors.

7. Validation and Verification.

The finite volume approach involves the numerical solution of partial differential equations involving RANS equations, resulting in the introduction of discretization inaccuracies. In terms of theory, there has been proposed that increasing the number of cells through discretization can minimize any inaccuracies. However, in the field of numerical analysis, it is necessary to investigate and analyze errors and uncertainties.

Solutions of fine, medium, and coarse mesh enhancement are denoted by the letters S_1, S_2 and S_3 respectively. Hence the convergence ratio,

$$R_G = \frac{\varepsilon_{21}}{\varepsilon_{32}} = \frac{S_2 - S_1}{S_3 - S_2} = 0.077$$

According to the conclusions of ITTC [ITTC, 2002], there exist three potential convergence possibilities:

i. Monotonic convergence: $0 < R_G < 1$
ii. Oscillatory convergence: $R_G < 0$

iii. Divergence: $R_G > 1$

Considering that the result is smaller than 1, the convergence is considered to be monotonic Convergence.

In this study, the systematic grid refinement ratio, r_g is $\sqrt{2}$ and, the P_{Gest} is 2 and it is an approximation of the order of precision decreases because the separation size approaches to zero. The order of accuracy p_G, first order of RE δ_{RE} correction factor C_G are determined below.

$$p_G = \frac{\ln(\varepsilon_{32}/\varepsilon_{21})}{\ln(r_g)} = 7.4$$

$$\delta_{RE} = \frac{\varepsilon_{21}}{r_g{}^{p_G} - 1} = 3.33 \times 10 - 7$$

$$C_G = \frac{r_g{}^{p_G} - 1}{r^{p_{Gest}} - 1} = 12.00$$

The uncertainty of the grid, denoted as U_G, is determined in the following manner:

$$U_G = |C_G \delta_{RE}| + |(1 - C_G)\,\delta_{RE}| = 7.67 \times 10^{-6}$$

The corrected solution can be determined by,

$$S_c = S_{G1} - \delta^*_{G1} = 4.236 \times 10 - 3$$

Where, $S_{G1} = S_1$

And, $\delta^*_{G1} = C_G \times \delta_{RE}$

The corrected answer has a precision of 99.91% in comparison to the original simulated outcome of S_1.

The error in comparison

$$E = S_1 - D = 5 \times 10^{-5} \;\; which \;\; is \;\; 1.16\%D.$$

Where, S_1 = Simulated Result of C_T at fine mesh

And, D = Experimental Result of C_T

The numerical uncertainty is determined using the following equation:

$$U_{SN} = \sqrt{U_G^2 + U_I^2}$$

Assuming that the iterative uncertainty (U_I) is much smaller than the grid uncertainty (U_G) (i.e., $U_I \ll U_G$), the overall uncertainty (U_{SN}) can be approximated as U.

$$U_{SN} = U_G = 7.67 \times 10^{-6} \;\; which \;\; is \;\; 0.18\%D.$$

To determine the validation uncertainty, the following equation that is presented below is used:

$$U_V = \sqrt{U_{SN}{}^2 + U_D{}^2} = 1.075 \times 10^{-4} \;\; which \;\; is \;\; 2.51\%D.$$

Here, experimental data uncertainty, U_D = 2.5% of D.

A tabular representation of the comparison error E, the validation uncertainty U_V, for the solution parameter may be found in Table 5.

Table 5: Comparison Error and Validation Uncertainty.

Result	|E| % D	U_V % D
C_T	1.16	2.51

Source: Authors.

As, $|E| < U_V$, according to Wilson [Wilson, et al., 2001] asserts that the fact that this criterion ($|E| < U_V$) exists indicates that the results have been successfully Validated.

Conclusions.

In the current investigation, numerical simulations are carried out in STAR-CCM+ which utilizes the Finite Volume Method (FVM) as its foundation to estimate resistance and resistance coefficient generated by a Japan Bulk Carrier (JBC) hull in calm water at Froude number 0.142. Additionally, a study on verification and validation is additionally carried out. The $k - \epsilon$ turbulence model with two equations is employed to provide the closure of the Reynolds Averaged Navier-Stokes (RANS) equation with the intention of obtaining pressure and velocity fields respectively. Volume of Fluid (VOF) is utilized to precisely identify the location of free surface between the multiphases. A comparison is made between the numerical results and the empirical findings that are currently accessible. The wave patterns accurately depict the Kelvin wave patterns whereas the wave elevation precisely mimics that observed in the experiment. To execute verification and validation study, three sets of grids that have been carefully enhanced and have specific a refinement ratio of $\sqrt{2}$ are developed as well as employed. The comparison errors to predict the resistance within the outcomes of the simulation along with the results of the experiment are less than two percent. The validation uncertainty, which is determined by considering both the numerical uncertainty alongside the experimental uncertainty, amounts to 2.51% of the EFD data. In contrast, the comparison error constitutes 1.16% of the EFD data. This indicates that the validation has been successfully accomplished and the modeling error is lower than the level of noise introduced by CFD and EFD. Additional refinement of the mesh can be performed in order to reduce the inaccuracies even further, but this will require a greater level of computing accessibility.

Acknowledgements.

The authors are thankful to Bangladesh University of Engineering and Technology for all of the assistances and supports.

References.

Farkas, A., Degiuli, N., & Martic, I. (2017). NUMERICAL SIMULATION OF THE VISCOUS FLOW AROUND a TANKER MODEL. *Brodogradnja*, *68*(2), 109–125. https://doi.org/10.21278/brod68208.

Gaggero, S., Villa, D., & Viviani, M. (2015). The kriso container ship (KCS) test case: an open source overview. *MARINE VI : Proceedings of the VI International Conference on Computational Methods in Marine Engineering*, 735–749. https://iris.unige.it/handle/11567/827299.

Hino, T., Stern, F., Larsson, L., Visonneau, M., Hirata, N., & Kim, J. (2020). Numerical Ship Hydrodynamics - An Assessment of the Tokyo 2015 Workshop. *Springer*. https://research.chalmers.se/en/publication/518565.

ITTC – Recommended Procedures and Guidelines 7.5 – 03 – 02 – 03, 2011, pp 11. https://ittc.info/media/1357/75-03-02-03.pdf.

ITTC Quality Manual, 7.5-03-01-01, (2002). "CFD General: Uncertainty analysis in CFD — Verification and validation methodology and procedures" . https://ittc.info/media/4184/75-03-01-01.pdf.

Khan, S., Gunpinar, E., & Sener, B. (2019). GenYacht: An interactive generative design system for computer-aided yacht hull design. *Ocean Engineering*, *191*, 106462. https://doi.org/10.1016/j.oceaneng.2019.106462.

Niklas, K., & Pruszko, H. (2019). Full-scale CFD simulations for the determination of ship resistance as a rational, alternative method to towing tank experiments. *Ocean Engineering*, *190*, 106435. https://doi.org/10.1016/j.oceaneng.2019.106435.

Richardson, L. F. (1911). IX. The approximate arithmetical solution by finite differences of physical problems involving differential equations, with an application to the stresses in a masonry dam. *Philosophical Transactions of the Royal Society of London Series a Containing Papers of a Mathematical or Physical Character*, *210*(459–470), 307–357. https://doi.org/10.1098/rsta.1911.0009.

Roache, P. J. (1998). *Verification and validation in computational science and engineering*. http://www.gbv.de/dms/goettingen/250414368.pdf.

Versteeg, H. K.; Malalasekera, W. An Introduction to Computational Fluid Dynamics: The Finite Volume Method; 2006 pp. 75-76.

Weller, HG (2008). "A new approach to VOF-based interface capturing methods for incompressible and compressible flow," Technical Report TR/HGW/04, OpenCFD Ltd.

Wilson, R. V., Stern, F., Coleman, H. W., & Paterson, E. G. (2001). Comprehensive Approach to Verification and Validation of CFD Simulations—Part 2: Application for RANS Simulation of a Cargo/Container Ship. *Journal of Fluids Engineering*, *123*(4), 803–810. https://doi.org/10.1115/1.1412236.

Yu, A., Wan, D., & Chen, G. (2019). Verification and validation for the resistance of a KRISO container ship in calm water. *The 29th International Ocean and Polar Engineering Conference*. https://onepetro.org/ISOPEIOPEC/proceedings/ISOPE-19/All-ISOPE19/ISOPE-I-19-029/20845.

Zhao, F., Zhu, S., & Zhang, Z. (2005). Numerical experiments of a benchmark hull based on a turbulent free-surface flow model. *Computer Modeling in Engineering & Sciences*, *9*(3), 273–286. https://doi.org/10.3970/cmes.2005.009.273.